JOURNAL OF CATALYSIS 42, 162–172 (1976)

Structure and Catalytic Activity of $MoO_3 \cdot SiO_2$ Systems

I. Solid State Properties

A. CASTELLAN, J. C. J. BART,[1] A. VAGHI, AND N. GIORDANO[2]

Montedison Research Centre, 20021 Bollate (Milan), Italy

Received November 8, 1974

Two series of $MoO_3 \cdot SiO_2$ catalysts (up to 25 wt% MoO_3), prepared by impregnation, but differing in calcination conditions at 500°C (presence or absence of steam), were subjected to a physicochemical investigation. In both series, the following species have been detected: silicomolybdic acid (SMA) and dimolybdate (DMA) up to 8 wt% MoO_3 coverage, polymolybdates PMA (max at 13% MoO_3) together with free MoO_3, as whiskers, at higher compositions. Incorporation of part of MoO_3 into the SiO_2 lattice is not excluded. Quantitative differences exist between the two series, with a larger fraction of SMA in the steam activated samples, at the expense of DMA; moreover, whiskers are larger and less numerous than in the absence of steam. To explain formation of whiskers, a mechanism has been proposed involving first reversible hydration of MoO_3 followed by interaction with silanol surface groups to form a silicomolybdic complex, which easily decomposes to give free MoO_3 due to its low stability. Morphological properties reveal discontinuities which are closely related to the onset of formation of different species; surface areas steadily decrease with increasing coverage, always exceeding variations expected from a monolayer deposition.

INTRODUCTION

In spite of considerable interest in the oxidation and ammoxidation of olefins over molybdate catalysts, so far little attention has been paid to catalytic properties of pure MoO_3 and to the influence of most common supports such as SiO_2. Some information on the catalytic properties of MoO_3 and/or $MoO_3 \cdot SiO_2$ is contained in work on the (amm)-oxidation of propylene (*1–9*) and oxydehydrogenation of butene (*10–12*). Generally speaking, pure MoO_3 is much less active than most molybdates. Reaction products are: acrolein (or acrylonitrile), acetaldehyde (or acetonitrile) and CO_x in the case of propylene; butadiene, products of isomerization and CO_x in the case of butenes. Although catalytic performance is strongly dependent upon experimental conditions, the general trend is towards an equivalent formation of CO_x and products of intermediate oxidation at least in the case of pure MoO_3. Work on the catalytic activity of $MoO_3 \cdot SiO_2$ is even less conclusive: attention has been focused here mostly on the study of solid state properties such as the process of reduction (*13*), reduction–reoxidation rates derived from EPR and electrical conductivity (*9, 14, 15*).

In view of the great industrial interest in $MoO_3 \cdot SiO_2$ systems we have now undertaken a systematic study aimed at isolating those properties of the solid which are most likely to be involved in the

[1] Present address: Montedison Research Laboratories "G. Donegani," Via del Lavoro 4, Novara, Italy.

[2] Present address: Istituto di Chimica Industriale, Università di Messina, Messina, Italy.

selective and complete oxidation of olefins. For this purpose microspheroidal SiO_2 of high surface area (SA) was loaded with up to 25 wt% MoO_3: results of these studies are discussed in the present work.

In a second paper (*16*) results of catalytic activity will be discussed; aspects related to the origin of various oxidation products and the underlying mechanisms will be dealt with in a third paper (*17*) where we also try to establish a link with active sites as disclosed in the present paper.

EXPERIMENTAL METHODS

Preparation of Samples

Catalysts were prepared by impregnation of microspheroidal SiO_2 (Ketjen, type F-5) with aqueous solutions of $(NH_4)_6Mo_7O_{24} \cdot 4H_2O$ (Kuhlmann) of concentrations leading to a final MoO_3 content from 2 to 25 wt%. After drying at 110°C overnight, catalysts were activated according to two different procedures: (a) calcination in a fluidized bed at 500°C for 4 hr in air saturated with 25 vol% water vapor (*V*-series); (b) calcination in an oven at 500°C for 8 hr in air (*A*-series). Reference to the various samples will be made by indicating their compositions as wt% MoO_3 followed by the designation of the series: thus MoO_3-2-*A* stands for 2 wt% MoO_3 activated in air.

The SiO_2 support used throughout was characterized by a total pore volume (V_t) of 1.1 cc/g, surface area (SA) of 633 m^2/g and average particle size (APS) of 50 μm.

Physicochemical Characterization

X-Ray powder analysis, optical microscopy, infrared and optical reflectance spectroscopy, surface area, porosimetric pore volume (V_p) and pore size distribution were determined as reported elsewhere (*18*). The total pore volume, V_t, was obtained by water titration.

Acidimetric titrations were performed to determine silicomolybdic acid (SMA). The method is based on the fact that the tetrabasic acid SMA presents two inflections on the neutralization curve, namely at pH 3.5 corresponding to the formation of a salt, $Na_4(SiMo_{12}O_{40})$ and at pH 10 in correspondence to the decomposition of the silicomolybdic anion, as follows:

$$(SiMo_{12}O_{40})^{4-} + 20\ OH^- \rightarrow 12\ MoO_4^{2-} + 10\ H_2O + SiO_2$$

The titrations were registered on a potentiograph (Metrohm E 436) in the range of pH 0–8 using glass–calomel electrodes. The region pH > 8 was not considered as contributing significantly to the knowledge of the various chemical species present, as in alkaline media other phenomena occur such as the neutralization of acidic substances with low dissociation constants and the decomposition of anionic (silicomolybdic and polymolybdic) complexes. In order to prevent solubilization of free MoO_3 and hydrolytic phenomena, anhydrous methanol was employed throughout as the solvent using CH_3ONa as a titrating agent. In this way, only MeOH-soluble substances are determined together with acidic compounds dispersed on the catalyst surface which are soluble as a sodium salt once a certain pH is reached.

RESULTS

Morphological properties of the *A*- and *V*-series (Table 1 and Figs. 1 and 2) indicate profound modifications of SiO_2 after impregnation and activation, which are most pronounced at higher MoO_3 contents (Fig. 1) and longer calcination times (Fig. 2). The experimental SA are lower than those calculated from the contribution of the support only, i.e., from simple dilution concepts. This holds both for the *A*- and the *V*-series even though the SA of the free support varies with the atmospheric conditioning due to the effect of steam; in fact, the initial SA value of the SiO_2-*V*-series is higher by 100 m^2/g (Fig. 1). Surface area as a function of the composition

TABLE 1

Morphological Properties of $MoO_3 \cdot SiO_2$

Composition	Surface area (m^2/g)	Total pore vol V_t (cm^3/g)	Porosimetric vol (V_p) (cm^3/g)	Av pore radius (Å) from:		Mean pore radius (Å)	$V_t - V_p$ (<37 Å)	Mean pore radius (%)		
				V_t	V_p			<37.5 Å	37.5–107 Å	>107 Å
SiO_2-*V*	729	0.93	0.65	25.5	17.8	~150	0.28	30.1	28.9	41
MoO_3-2-*V*	679		0.60		17.7	~180				
4-*V*	664	0.78	0.47	23.5	14.2	~150	0.31	39.7	26.0	34.3
6-*V*	529		0.39		14.7	~140				
8-*V*	566	0.76	0.42	26.9	14.8	~140	0.34	44.7	25.0	30.3
10-*V*	536		0.38		14.2	~150				
13-*V*	393	0.71	0.53	36.1	27.0	~107	0.18	25.4	37.6	37.0
16-*V*	294		0.58		39.5	~60				
20-*V*	260	0.71	0.46	54.6	35.4	~53	0.25	35.2	44.4	20.8
23-*V*	242		0.44		36.4	~51				
25-*V*	208	0.57	0.52	54.8	50.0	~55	0.05	8.8	66.4	24.8

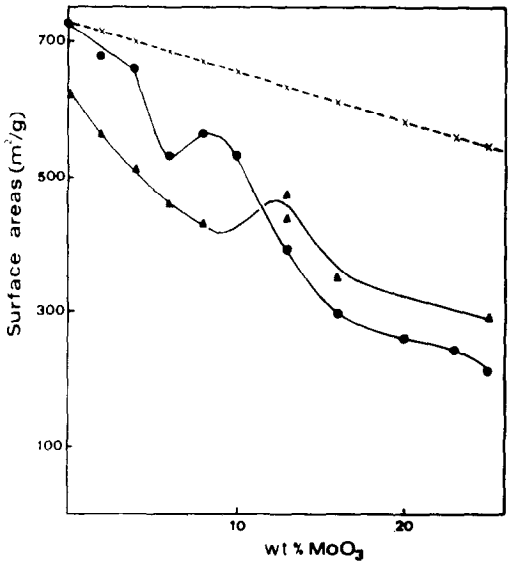

FIG. 1. Surface areas (m^2/g) of $MoO_3 \cdot SiO_2$ catalysts as a function of the composition (●) *V*-series; (▲) *A*-series. (– – –) theoretical value calculated from the weight fraction of the pure support.

(Table 1, Fig. 1) clearly reveal some discontinuities at MoO_3-6-*V* and MoO_3-10-*A*, leading ultimately to higher values for the *A*-series in the MoO_3-richest region (Fig. 1). Discontinuities are also evident: (a) in the average pore radii which almost double at MoO_3-13-*V* (Table 1); (b) in the pore size distribution drifting in the manner illustrated in Table 1 for the V-series (last three columns). We thus observe: (i) increase of pore volumes with radii <37 Å up to a maximum at MoO_3-8-*V* with decrease afterwards; (ii) pore volumes in the range 37–107 Å constant up to MoO_3-8-*V* followed by a sharp increase at higher compositions; (iii) a steady decrease of pore volumes in the range >107 Å. Altogether, these results indicate that below a certain composition (MoO_3-8-*V*) more micropores are formed than are originally present in the support. Subsequently enlargement of existing pores occurs as is also proven by the similarity in the hysteresis profiles of the adsorption–desorption isotherms of N_2 on SiO_2 and MoO_3-25-*A*

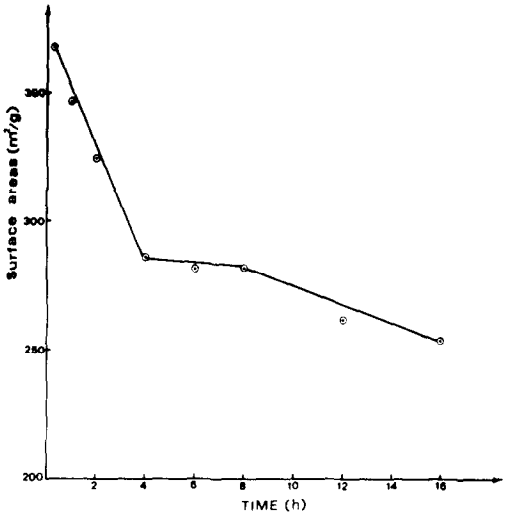

FIG. 2. Variations in surface area (SA) of MoO_3-23-*A* with calcination time at 500°C.

taken as a reference (Fig. 3); the shape of these isotherms indicates that pores are of the ink bottle type (*19*).

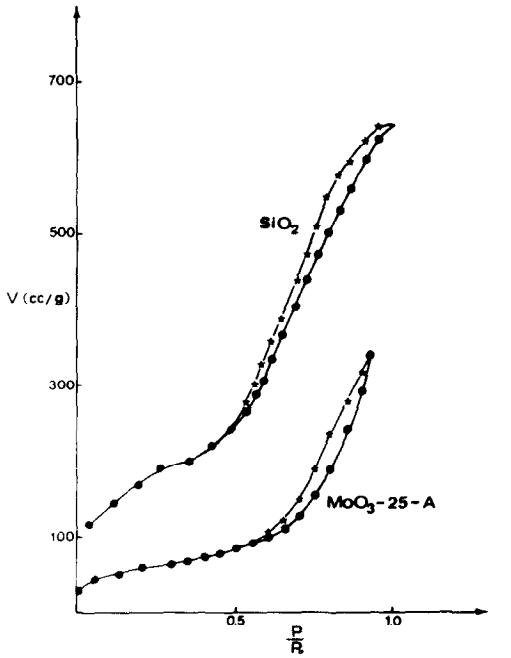

FIG. 3. Hysteresis profiles of adsorption–desorption isotherms of N_2 on SiO_2 and MoO_3-25-*A*. Adsorption (●); desorption (★), measured in a BET-type apparatus (Sorptomatic C. Erba).

The discontinuities found in the morphological properties are further substantiated by results of other techniques. Thus in X-ray patterns onset of "free" MoO_3 is detected at MoO_3-13-*V* as against MoO_3-17-*A*. No diffraction bands other than those of MoO_3 were observed. These results agree with observations in the optical microscope: MoO_3 has the form of prismatic lamellar crystals ($\bar{n}_{Li} = 2.5$) external to the SiO_2 granules; because of their origin and shape these crystals are indicated as whiskers.

In the *A* series, whiskers are smaller in size but more numerous than in the *V*-series (see Plates 1 and 2). Besides, observations under bright-field revealed the presence of yellow MoO_3-like structures enveloping the SiO_2 granules: leaching with water or CH_3OH removes this yellow phase. Microanalysis of the aqueous or alcoholic extract indicated the presence of both Si^{4+} and Mo^{6+} in the low MoO_3 region (MoO_3-8-*A*) and of almost exclusively Mo^{6+} at higher compositions (MoO_3-23-*A*). Attack of these leached granules by NH_4OH (to remove MoO_3) and subsequently by H_2O_2 caused renewal of the yellow coloration (due to peroxocomplexes) most pronounced in the MoO_3-23-*A* sample: it points to Mo^{6+} strongly bound to SiO_2, thus differing from whiskers and the extractable yellow phase. Differences also arise as a function of the time of activation. Thus with increasing calcination time, a MoO_3-8-*A* sample at 500°C showed incipient submicroscopic crystallizations followed by onset of whisker formation at longer times (25 hr). A similar treatment applied to MoO_3-23-*A* indicated formation of whiskers already after 15 min; the latter slowly segregate from the bulk of the granules (2–4 hr) until they become well separated at longer times. The evolution of SA with time (Fig. 2) reflects this behavior as it indicates two processes: (a) an initial drop due to

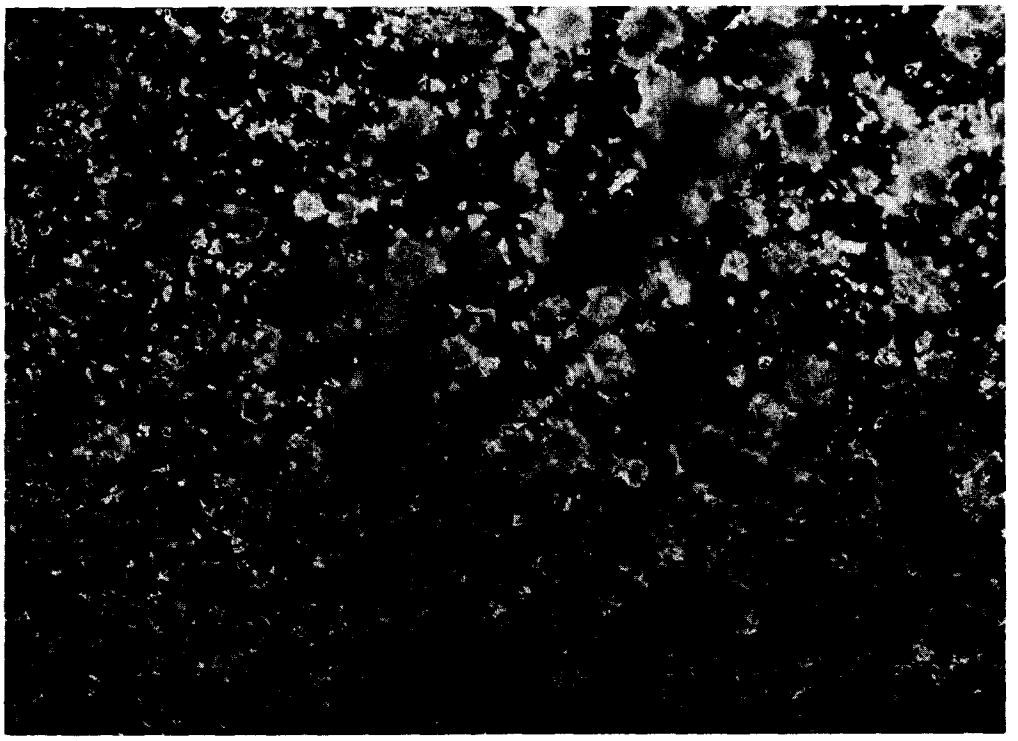

PLATE 1. MoO_3–25-*A* at 105× magnification in dark field.

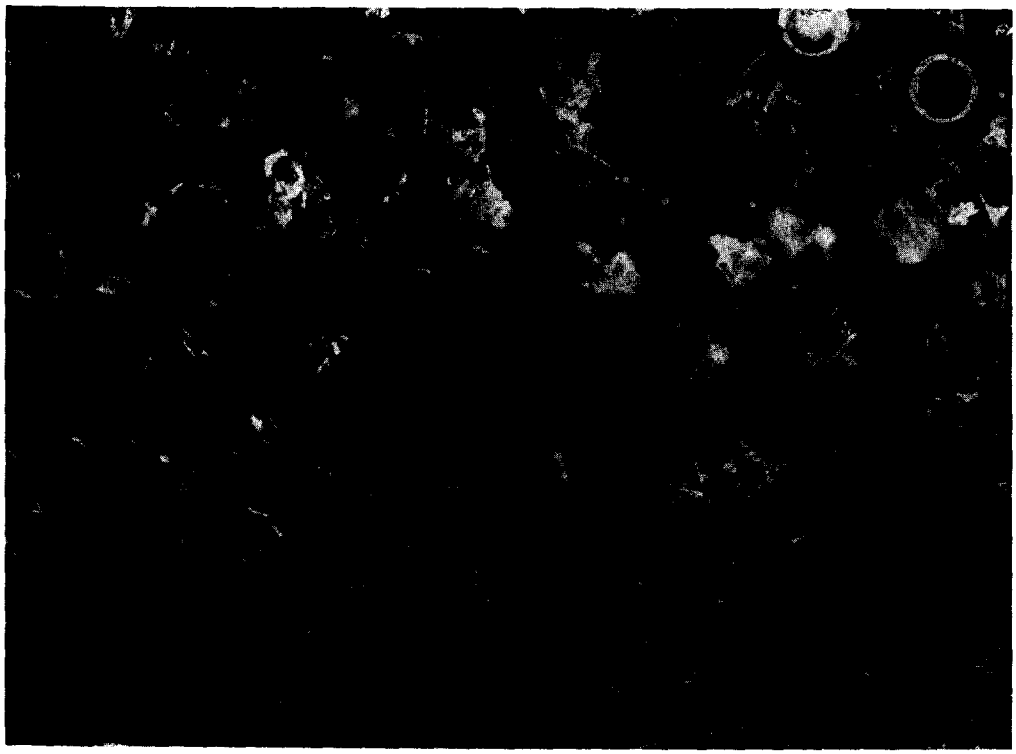

PLATE 2. MoO_3-25-*V* at 105× magnification in dark field.

sintering and (b) uncovering of pores and surface area beneath, due to segregation of whiskers leading ultimately to a plateau at 4–8 hr. Details of this behavior are discussed elsewhere (*20*).

Electronic spectra also depict the variations with composition and activation conditions. Samples of the *V*-series (Fig. 4) display maxima at 265 nm (A_1) and 305 nm (A_2) with the latter shifting up to 325–330 nm as the MoO_3 content increases; the ratio of absorbances A_2/A_1 increases with the composition. The *A*-series (Fig. 5) is mainly characterized by a single band, A_2, which shifts gradually from 280 to 330 nm, the absorption at 265 nm (A_1) not being clearly distinguishable. In both series, the absolute intensity of the absorbance increases with the MoO_3 content up to MoO_3-13-*V* and 16-*A*, respectively; the decrease at higher MoO_3 contents is due to lower surface areas and/or changes in the nature of the surface structures.

The 265 nm band can be assigned to tetrahedral Mo(VI), as in Na_2MoO_4 (*21*, *22*). As to the absorption at higher wavelengths (λ) more than one possibility arises: octahedral Mo(VI) as in polymolybdates or MoO_3 which absorb at 305 nm (*22*) or 327 nm (*23–25*) and molybdenyl species absorbing at 325–340 nm (*23–25*). Clearly in the *V*-series tetrahedral Mo(VI) is important at the lowest MoO_3 compositions (2–4%) as $A_1/A_2 \cong 1$; at higher compositions, the decreasing A_1/A_2 ratio and the shift of the maximum toward higher λ suggests more octahedral Mo(VI) either as in polymolybdates or in MoO_3 or as molybdenyl species. The *A*-series behaves similarly: distinctive features are fewer tetrahedral Mo(VI) species and a more gradual shift towards species of the octahedral type.

The interpretation of the ir spectra is made difficult by superposition of characteristic absorption bands of MoO_3 and SiO_2.

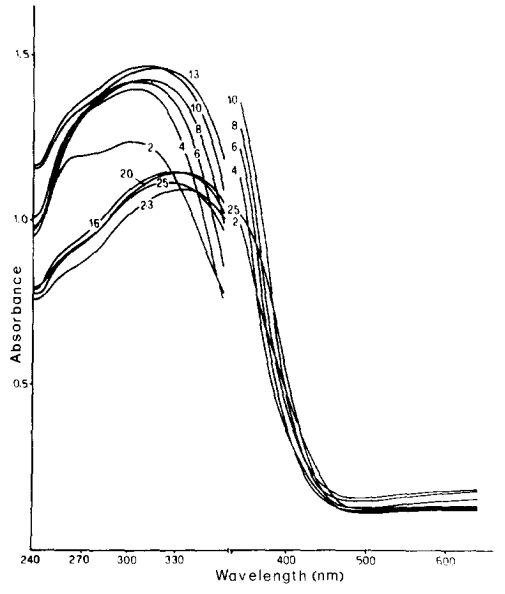

FIG. 4. Optical reflectance spectra of $MoO_3 \cdot SiO_2$ samples (*V*-series). Numerals refer to wt% MoO_3; absorbance on absolute scale.

Nevertheless, the intensity of the 360 cm^{-1} band, attributable to bending of the O_1–Mo–O_2 bonds in MoO_3 (*26*) varies with composition in the way already described in the results from X-ray diffraction

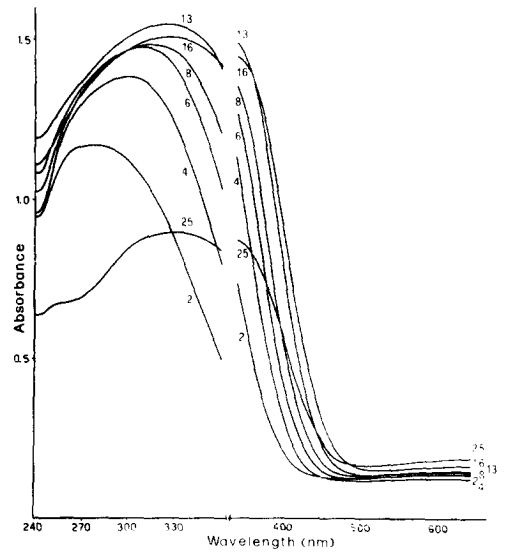

FIG. 5. Optical reflectance spectra of $MoO_3 \cdot SiO_2$ samples (*A*-series). Numerals refer to wt% MoO_3; absorbance on absolute scale.

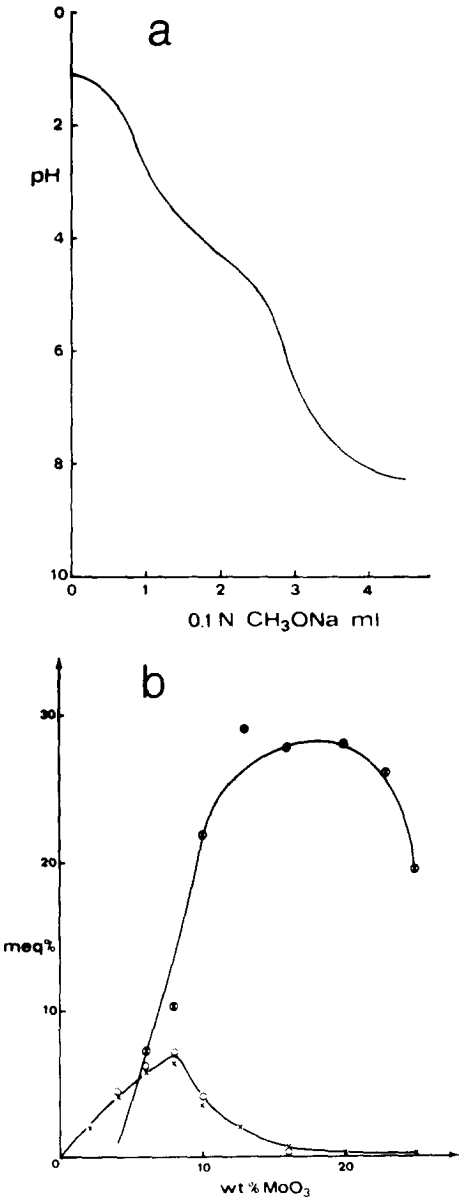

FIG. 6. (a) Acidimetric titration of a methanol solution of MoO_3–SiO_2 catalysts with 0.1 *N* CH_3ONa. (b) Meq% of SMA (×) and (○) and PMA (⊗) from acidimetric titration of $MoO_3 \cdot SiO_2$ catalysts (*V*-series).

and optical microscopy. Differences between the *V*- and the *A*-series were also confirmed.

Results of acidimetric titration gave useful information as to the nature of

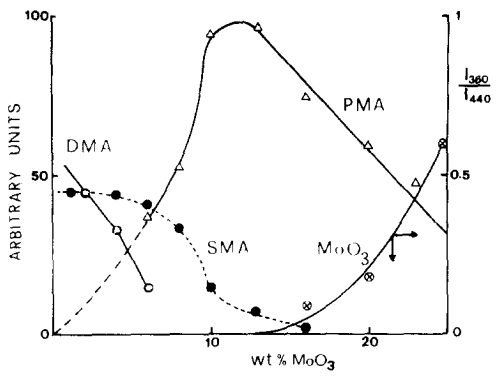

FIG. 7. Product distribution in $MoO_3 \cdot SiO_2$ catalysts in fractional units as a function of the composition, as determined from acidimetric titrations: silicomolybdic acid (SMA) (●); (di)molybdates (DMA) (○); polymolybdates (PMA) (△). The estimate of the MoO_3 fraction (⊗), in arbitrary units, is derived from the intensity ratio of the ir reflectance bands at 360 and 440 cm^{-1}.

various molybdenum species. The titration with CH_3ONa in the presence of the solid suspended in anhydrous CH_3OH is of the type illustrated in Fig. 6a with two inflections at pH = 2.5 and 6. Excluding MoO_3 and SiO_2, both insoluble in CH_3OH, various other species were considered among which was SMA. This attribution proved to be correct as the analysis of the methanolic solution, following rapid extraction in a Soxhlet apparatus, have a single inflection at pH 2.5 and a Mo:Si ratio as in SMA. As to the second inflection, this was attributed to polymolybdic acids (PMA) obeying the equilibrium:

$$xMoO_4^{2-} + nH^+ \rightleftarrows [Mo_xO_y]^{m-} + n/2H_2O.$$

Review of the literature (*27*) reveals that at pH 6, species in equilibrium may range from $Mo_3O_{11}^{4-}$ (pH 6.5) to $Mo_7O_{24}^{6-}$ (pH 4.8). Product distribution as a function of the composition is illustrated in Figs. 6b and 7, respectively, in terms of meq% and fraction of Mo bound as SMA or PMA.

To gain further information on the system, samples of MoO_3-25-*A* were treated as follows: (a) in an apparatus for the determination of the attrition resistance (Roller-Aminco) to free the granules from whiskers (the residual sample containing 20% MoO_3 is designated as B); (b) with NH_4OH solution (3%) to dissolve free molybdenum species only (*28*) (the residual sample containing 8% MoO_3 is designated as C). Differences with respect to the reference sample (MoO_3-25-*A*) were explored by different techniques. Thus uv spectra (Fig. 8) showed increase of the absorbance intensity both for the B and the C series and a shift of λ_{max} toward lower λ, i.e., from 328 (A) to 310 (B) and 290 mm (C). These features are in line with previous observations indicating presence of whiskers on the surface which are easily removable by simple mechanical or chemical treatment; the position of λ_{max} indicates that products of profound interaction with the SiO_2 support exhibit essentially a tetrahedral Mo coordination. The near ir region (omitted in Fig. 8) shows

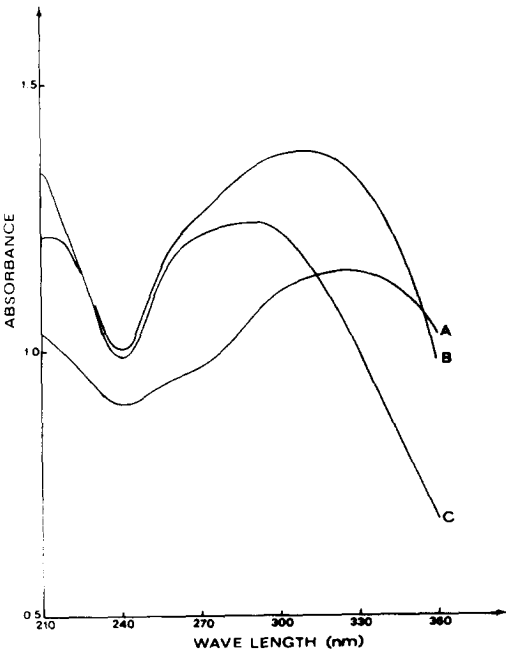

FIG. 8. Optical reflectance spectra of MoO_3-25-*A* before (A) and after (B) the determination of attrition resistance; (C) refers to MoO_3-25-*A* after treatment with NH_4OH (3%).

bands at 1400 and 1900 nm due to OH or H_2O (*29*), a 1000 nm band due to Mo(VI) and a weak one at 700 nm [Mo(V) being most pronounced in the C-series]. Surface areas were, respectively: 254 m^2/g (A), 253 m^2/g (B), and 284 m^2/g (C).

DISCUSSION

Generally speaking, impregnation of a support by active elements can give rise to products of physical and/or chemical interactions. Thus in the present case we may envisage MoO_3 to be uniformly deposited over the surface as a monolayer (monophase model) or in the form of clusters (biphase model). Moreover, one can expect more or less well-defined compounds as a result of chemical interaction of MoO_3 with SiO_2.

A discrimination among various possibilities is offered partly by the morphological properties, i.e., surface areas and pore volumes, which are significantly lower than expected from the contribution of the unloaded support (Fig. 1 and Tab. 1): consequently, it is suggested that profound modifications have occurred through chemical interaction. This simple picture will be illustrated in detail in the following discussion, by considering separately the two compositional regions into which the system can formally be divided.

In the *V*-series, the main feature of the low MoO_3 region (up to the MoO_3-10) is the presence of SMA with a maximum at MoO_3-8 (Fig. 6b); Fig. 7 further indicates that SMA accounts for about half of the total molybdenum content. The presence of SMA explains well the modifications in morphological properties, such as the presence of more micropores than in the original SiO_2: Table 1 indicates in fact that the maximum content of the pores of $r < 37$ Å occurs at MoO_3-8. Nevertheless, on the basis of the results of Fig. 7, SMA is not the only species present: from spectroscopic evidence it is suggested that the balance with respect to SMA is attributable to Mo(VI) in tetrahedral coordination. Clearly, the latter species may arise from interaction between molybdic acid and hydroxyl surface groups of SiO_2 according to:

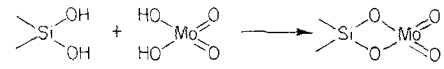

in much the same manner as already described for the $MoO_3 \cdot Al_2O_3$ system (*18, 30*). There is, however, a quantitative difference since on SiO_2 tetrahedral Mo(VI) is confined to the lowest compositions whereas it is much more abundant (up to MoO_3-10) in the Al_2O_3-based systems.

Compositions above MoO_3-10 are characterized by "free" MoO_3 and some surface-bound species, among which are polymolybdic acids (PMA) as is evident from the inflections at pH 6 in the acidimetric titrations: quantitatively PMA presents a broad maximum between 12 and 20% MoO_3 (Fig. 6b) whereas, on a fractional basis it displays a sharp maximum at MoO_3-12 (Fig. 7). At this composition, PMA constitutes the only species present besides minor amounts of SMA (Fig. 7). Presence of PMA is also suggested by the 305 nm band in the electronic spectra (Fig. 4). Further rise in MoO_3 content ($> MoO_3$-13) leads to an increasing incidence of "free" MoO_3, as is evident from X-ray diffraction, optical microscopy and ir spectra, all indicating a rather steep increase of MoO_3 as a function of the composition. Neither PMA nor MoO_3, however, satisfactorily explain the observed strong decrease of SA, exceeding that in the low MoO_3 region. Most likely, products of more profound interaction (i.e., Mo^{6+} in the Si^{4+} lattice) appear to coexist, as suggested for the C-sample by the abundance of Mo(VI) in tetrahedral coordination, larger than in its formally equivalent sample (cf. Figs. 4 and 8); similar suggestions are derivable from SA (284 m^2/g) which is much lower than in the reference sample (566 m^2/g for

the MoO_3-8-*V* sample). Further evidence may be added from the massive presence of cristobalite in samples based on SiO_2–gel (Ludox) and activated at 600°C (*20*).

The role of steam as a variable in the activation process becomes clear if we consider that the main difference between the two series of catalysts is the size and amount of whiskers. To explain this observation, we assume, first, reversible hydration of MoO_3:

$$(MoO_3)_{surface} + xH_2O \rightleftharpoons (MoO_3 \cdot xH_2O)_{surface}, \quad (I)$$

similar to the well-known promoting effect of water on the formation of various molybdates (*31*, *32*). The second step would involve reaction of molybdic acid with the silanol surface groups of the SiO_2 support to form a silicomolybdic complex:

$$(MoO_3 \cdot xH_2O)_{surface} + \begin{array}{c}|\\ -Si-OH\\ |\end{array} \xrightarrow[110\text{–}400°C]{} (MoO_3 \cdot SiO_2 \cdot H_2O)_{complex}. \quad (II)$$

Formation of whiskers may derive from decomposition of this complex, also in accordance with its low stability (*33*). This sequence of events agrees with optical observations indicating formation of whiskers at the expense of the yellow phase (SMA) enveloping the granules. According to this scheme, steam acts through: (i) the number of points of attack, regulating the equilibrium of Eq. (I) and the OH concentration of the SiO_2 surface; (ii) the rate of decomposition of the complex in Eq. (II); (iii) the rate of whisker growth. Three aspects explain well the observation of larger and less numerous whiskers in the *V*-series as opposed to the *A*-series. The above considerations also explain the onset of MoO_3 only at the higher compositions: thus, once SMA reaches a high concentration, it starts to decompose more quickly, or, stated differently, its stability approaches that of free SMA.

CONCLUSIONS

The results described above clearly demonstrate the active role of so-called "inert" supports on the formation of well-defined chemical species which may eventually be sites of catalytic activity. This paper shows how interaction of MoO_3 with a commercial silica support leads to MoO_4^{2-} and to silicomolybdic acid at low concentrations of the active element (max 8 wt%), as well as to polymolybdates (max 13 wt%) and to MoO_3 whiskers (>13 wt%). Finally, also incorporation of molybdenum into the lattice of the support is not excluded *a priori*.

ACKNOWLEDGMENTS

Thanks are due to Dr. L. Mariani for expert analytical chemical assistance and to Dr. A. Marzi for optical microscopy.

REFERENCES

1. Gel'bshtein, A. I., Stroeva, S. S., Kul'kova, N. V., Bakshi, Y. M., Lapidus, V. L., Vasil'eva, I. B., and Sevast'yanov, N. G., *Neftekhimiya* **4**, 906 (1964).
2. Moro-oka, Y., Tan, S. and Ozaki, A., *J. Catal.* **12**, 291 (1968).
3. Buiten, J., *J. Catal.* **10**, 188 (1968).
4. Sachtler, W. M., and De Boer, N. H., Proc. Int. Congr. Catal., Amsterdam (1964), I, 252.
5. Stroeva, S. S., Gel'bshtein, A. I., Kul'kova, N. V., Shscheglova, G. G., Ezhkova, Z. I., and Roginskaya, Y. E., *Neftekhimiya* **6**, 412 (1966).
6. Kutseva, L. N., and Margolis, L. Ya,. *Zh. Obshch. Khim.* **32**, 102 (1962).
7. Trifirò, F., and Pasquon, I., *Chim. Ind.* (*Milano*) **53**, 577 (1971).
8. Trifirò, F., and Pasquon, I., *J. Catal.* **12**, 412 (1968).
9. Peacock, J. M., Parker, A. J., Ashmore, P. G., and Hockey, J. A., *J. Catal.* **15**, 398 (1969).
10. Batist, P. A., Lippens, B. C., and Schuit, G. C. A., *J. Catal.* **5**, 55 (1966).
11. Mal'yan, A. N., Bakshi, Y. M., and Gel'bshtein, A. I., *Kinet. Katal.* **9**. 585 (1968).
12. Batist, P. A., Kapteijns, C. J., Lippens, B. C., and Schuit, G. C. A., *J. Catal.* **7**, 33 (1967).
13. Dufaux, M., Che, M., and Naccache, C., *J. Chim. Phys. Physicochim. Biol.* **67**, 527 (1970).

14. Sancier, K. M., Dozono, T., and Wise, H., *J. Catal.* **23**, 670 (1971).
15. Peacock, J. M., Parker, A. J., Ashmore, F. G., and Hockey, J. A., *J. Catal.* **15**, 387 (1969).
16. Vaghi, A., Castellan, A., Bart, J. C. J., and Giordano, N., *J. Catal.* (in press).
17. Giordano, N., Meazza, M., Castellan, A., Bart, J. C. J., and Ragaini, V., unpublished data.
18. Giordano, N., Bart, J. C. J., Vaghi, A., Castellan, A., and Martinotti, G., *J. Catal.* **36**, 81 (1975).
19. De Boer, J. H., *in* "The Structure and Properties of Porous Materials" (D. H. Everett and F. S. Stone, Eds.). Butterworths, London, 1958.
20. Marzi, A., Bart, J. C. J., Castellan, A., and Giordano, N., unpublished data.
21. Ashley, J. H., and Mitchell, P. C. H., *J. Chem. Soc. A* 2821 (1968).
22. Ashley, J. H., and Mitchell, P. C. H., *J. Chem. Soc. A* 2730 (1969).
23. Asmolov, G. N., and Krylov, O. V., *Kinet. Katal.* **11**, 1028 (1970).
24. Mitchell, P. C. H., and Trifirò, F., *J. Chem. Soc. A* 3183 (1970).
25. Bartecki, A., and Dembicka, D., *J. Inorg. Nucl. Chem.* **29**, 2907 (1967).
26. Mattes, R., and Schröder, F., *Z. Naturforsch. B* **24**, 1095 (1969).
27. Tsigdinos, G. A., and Hallada, C. J., Molybdenum Chemicals-Chemical Data Series Bulletin, 14 Feb. 1969.
28. Ishii, Y., and Matsuura, I., *Technol. Rep. Kansai Univ.* **10**, 47 (1969).
29. Anderson, J. H., and Wickersheim, K. A., *Surface Sci.* **2**, 252 (1964).
30. Giordano, N., Bart, J. C. J., Castellan, A. and Vaghi, A., *in* "Proceedings of the First International Conference on the Chemistry and Uses of Molybdenum" (Reading, 1973), (P. C. H. Mitchell, Ed.), p. 194. Climax Molybdenum Co., London, 1973.
31. Callahan, J. L., Petrucci, R. H., and Brown, C. A., *J. Colloid Chem.* **15**, 418 (1960).
32. Tammann, G., and Westerhold, F., *Z. Anorg. Allg. Chem.* **149**, 21 (1925).
33. West, S. F., and Audrieth, L. F., *J. Phys. Chem.* **59**, 1069 (1955).